Journal of Materials Chemistry A

ROYAL SOCIETY OF CHEMISTRY

COMMUNICATION

View Article Online
View Journal | View Issue

Cite this: *J. Mater. Chem. A*, 2020, **8**, 14921

Received 3rd June 2020
Accepted 8th July 2020

DOI: 10.1039/d0ta05568a

rsc.li/materials-a

Suppression of hydrogen evolution at catalytic surfaces in aqueous lithium ion batteries†

Fei Wang,‡*[a] Chuan-Fu Lin,‡[bc] Xiao Ji,‡[d] Gary W. Rubloff[b] and Chunsheng Wang*[de]

Aqueous lithium ion batteries (ALIBs) have attracted increasing attention due to their excellent safety profile. The water-in-salt electrolyte (WiSE) has enabled a wider voltage window (3.0 V) through the formation of an solid–electrolyte–interphase (SEI) on the anode. However, the cathodic limit of the WiSE and its derivatives cannot effectively support the desired energy-dense anodes, such as $Li_4Ti_5O_{12}$ (LTO). At the anode, the hydrogen evolution reaction (HER) is the main parasitic process that competes with the desired lithiation process therein. We investigated the catalytic activity of different coating layers and postulated the selection criterion for the surface layers. We demonstrated that Al_2O_3 had a surface that effectively suppressed the HER and enabled the cycling of the LTO anode in the WiSE, thereby delivering a capacity of 145 mA h g^{-1}. Such understanding provides important guidelines for designing electrolytes and interphases for aqueous battery chemistries.

Aqueous lithium ion batteries (ALIBs) are a promising type of energy-storage technology due to their non-flammable nature, the capability to be manufactured in an ambient environment, and the low reliance on battery-management systems at module or pack levels.[1–5] However, traditional ALIBs are limited by their inferior energy densities, which is caused primarily by the narrow window of electrochemical stability of water (1.23 V).[3,6] Recently, the expanded stability window (3.0 V) of the "water-in-salt" electrolyte (WiSE) overcame this restriction and enabled a series of high voltage/energy aqueous battery chemistries that were once prohibited in aqueous systems.[4,7–10] Expansion of the cathodic limit by 0.6 V was realized by the formation of a solid–electrolyte–interphase (SEI) on the anode surface derived from the reduction of salt anions and overall reduction of water activity.[9,11] However, the cathodically polarized anode surface would repel the anions away from the inner-Helmholtz layer of the surface, so further expansion of the cathodic limits *via* anion reduction becomes very challenging even with a higher concentration.[11,12] Hence, the cathodic limit of the WiSE is still not low enough to support anode materials such as $Li_4Ti_5O_{12}$ (LTO), whose redox potential is 1.55 V compared with that of Li, and sits near the cathodic limit of the WiSE.[13]

The passivation capability of the SEI formed in most non-aqueous electrolytes enables a cathodic stability limit well below 1.0 V, which is obviously more effective than anion-derived SEIs formed in the WiSE.[14–18] Apparently, the chemical nature of the SEI is critical for expansion of the stability window of the electrolyte. The primary criterion for an effective SEI is its electrolyte nature (*i.e.*, insulating electrons while conducting ions of importance to the cell reactions[17,19–22]). For aqueous systems, this criterion can be translated into low catalytic activity for the hydrogen evolution reaction (HER) because the latter is the main parasitic process at the anode and competes with the desired lithiation process therein. Suppressing the HER catalytic activity of the zinc metal anode in aqueous batteries helps to avoid water decomposition.[23–26] Kinetic suppression of the HER of the LTO anode is rarely investigated from the battery perspective. Conversely, the HER has been investigated intensely for splitting water electrochemically, the behavior of which is represented by volcano plots.[27–35] Thus, reverse use of volcano plots could help us find materials that are least catalytic for the HER which, in theory, could serve as an electrode surface friendly to SEI growth.

Guided by the theoretical calculation using the Gibbs free energy for atomic hydrogen adsorption (ΔG_H) and density of states (DOS), we investigated the electrochemical performances of uncoated Al_2O_3 and ZnO, and TiO_2-coated LTO electrodes in

[a]*Department of Materials Science, Fudan University, Shanghai, 200433, China. E-mail: feiw@fudan.edu.cn*

[b]*Department of Materials Science and Engineering, University of Maryland, College Park, MD 20742, USA*

[c]*Department of Mechanical Engineering, The Cathode University of America, Washington, DC 20064, USA*

[d]*Department of Chemical and Biomolecular Engineering, University of Maryland, College Park, MD 20742, USA. E-mail: cswang@umd.edu*

[e]*Department of Chemistry and Biochemistry, University of Maryland, College Park, MD 20742, USA*

† Electronic supplementary information (ESI) available. See DOI: 10.1039/d0ta05568a

‡ F. Wang, C. Lin and X. Ji contributed equally to this work.

the WiSE. We demonstrated that Al_2O_3 has a surface that effectively suppresses the HER and enables the cycle of the LTO anode in WiSE, delivering a capacity of 145 mA h g^{-1}. This selection criterion for a SEI-friendly surface in an aqueous electrolyte provides a novel approach to engineer interphases for next-generation battery chemistries.

When evaluated as the electrode substrate in the WiSE, various metallic current collectors demonstrated completely different limits of cathodic stability, which (as determined by the HER potentials) increased in the order Al < Ti < SS < carbon < Cu < Ni (Fig. S1†), and were in accordance with the volcano plot reported for the HER on metal electrodes. This observation suggests that there should be a correlation between metal-surface passivation and the reduction in their catalytic activities.[28,34] In particular, the reduction onset potential for Al was significantly lower than that of the others, indicating a possible combined contribution of its inherent low catalytic activity and dense surface passivation. Typically, the window of electrochemical stability of electrolytes is assessed using the linear sweep method on non-porous electrode surfaces, but this window varies significantly with the electrode materials. This difference can be pronounced, especially if the electrode materials used are composites, such as those in real-life electrochemical devices,[36] where an appreciable amount of conductive carbon and polymer binder lead to much higher surface area and catalytic activities than those in non-porous metal surfaces. Hence, the actual reduction or oxidation stabilities of an electrolyte in those devices will be affected largely by the surface properties of the carbon and active materials, with a minor contribution from the current collectors.

The HER is a surface reaction that is heavily dependent upon the interaction between the adsorbed hydrogen atom (H_{ads}) and the catalytic activity of the electrode surface (Fig. 1a).[31,35,37] Thus, to improve the performance of a battery anode in aqueous electrolytes, one must attempt the exact opposite of electrocatalysis: make the electrode surface as minimally catalytic as possible. Based on this *rationale*, we sought to apply materials of "poor" catalytic activity as a conformal coating on an electrode, which served to physically prevent direct contact between the electrolyte and electrode.

Using density functional theory (DFT), we calculated the free energy of hydrogen (ΔG_H) on various coating materials as well as their electronic conductivity, and used these two parameters to screen for the best candidate material. Materials with suitable hydrogen adsorption (neither too strong nor too weak) located at the top of volcano plots would have optimum activity. Hence, materials with either very strong (highly negative $-\Delta G_H$)

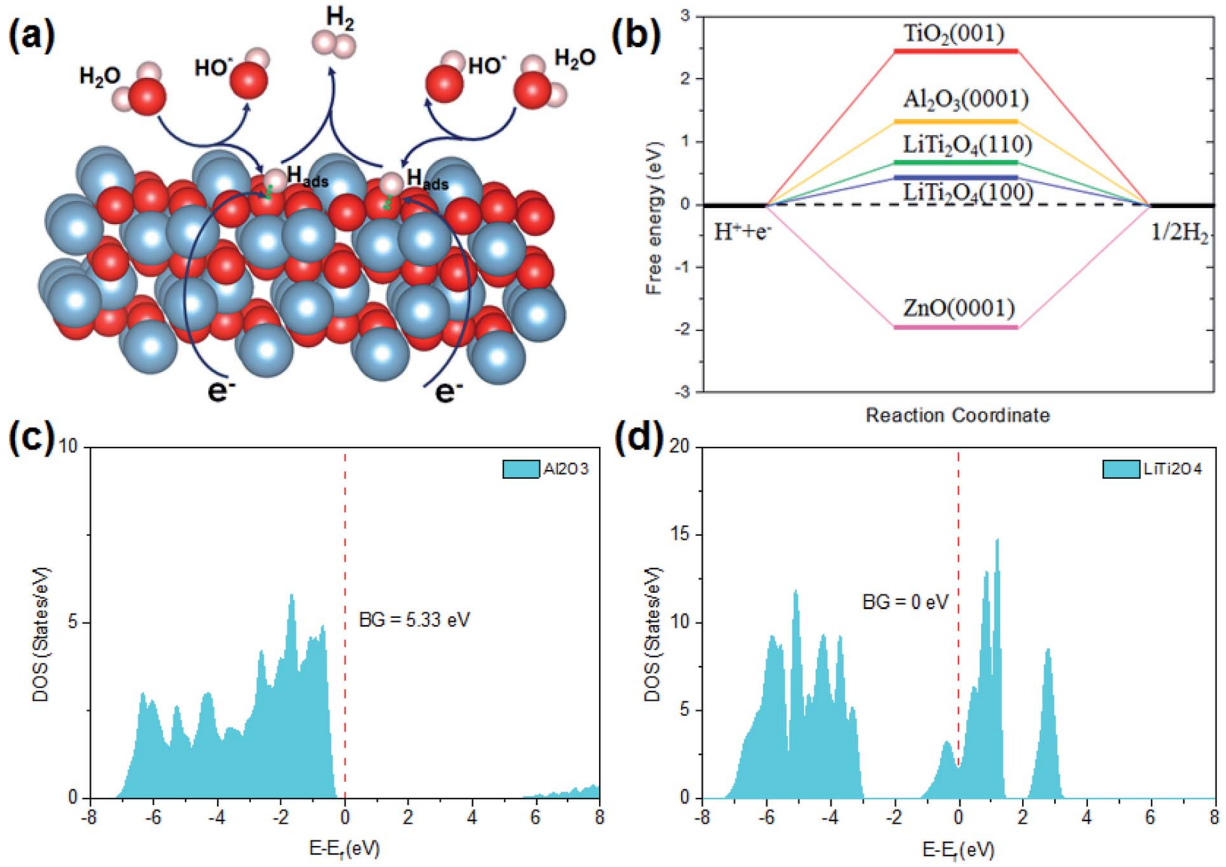

Fig. 1 (a) The HER process on electrode/electrolyte interfaces (schematic). (b) Simulation results of the free energy of adsorption of hydrogen (ΔG_H) for the different surface coatings. The density of state for (c) Al_2O_3 and (d) $LiTi_2O_4$. The red dashed lines indicate Fermi energies, and the bandgaps (BG) are listed.

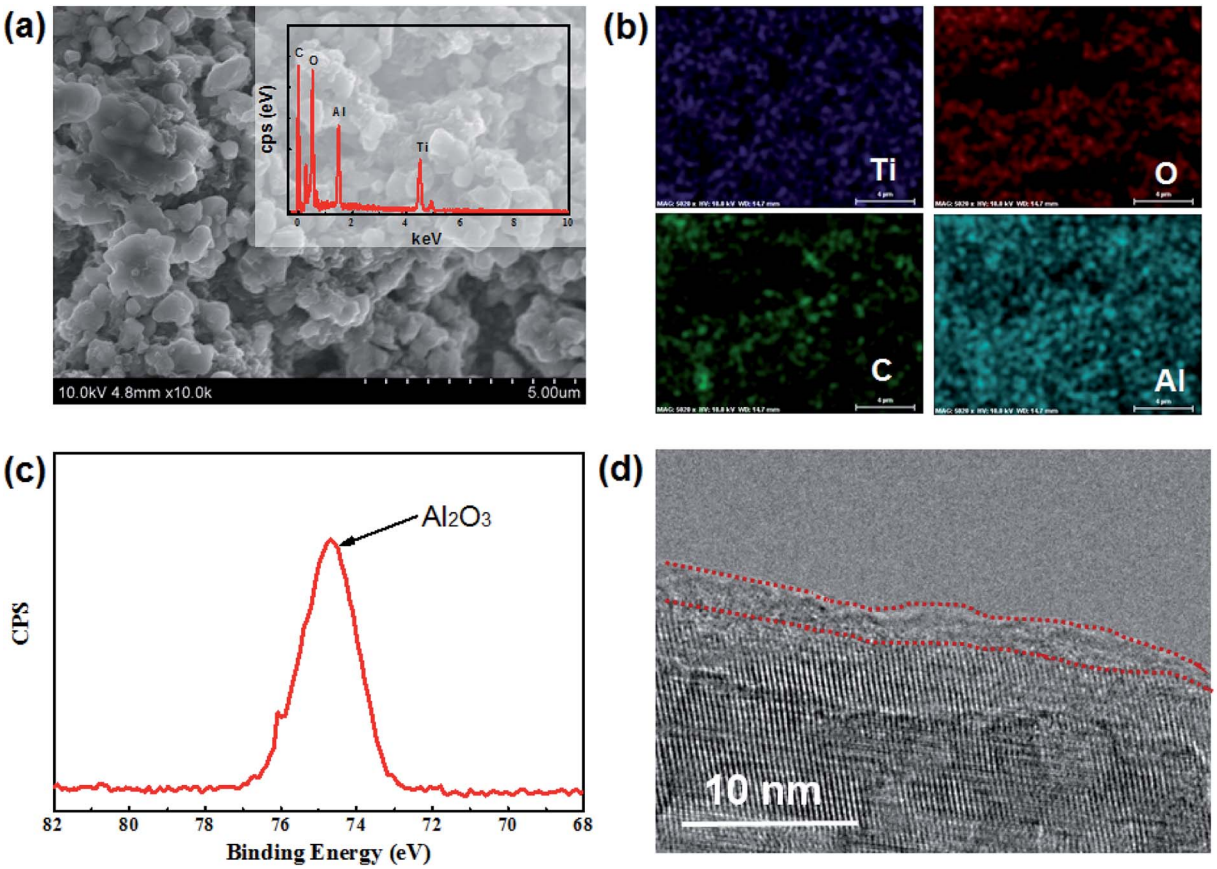

Fig. 2 (a) SEM image of the Al_2O_3-coated LTO electrode and corresponding EDX results. (b) Element mapping, (c) Al-XPS spectra and (d) TEM image of the Al_2O_3-coated LTO electrode.

or very weak bonding (highly positive $+\Delta G_H$) should be ideal candidates to suppress the HER. The high ΔG_H of Al_2O_3 (Fig. 1b) suggested its suitability whereas TiO_2, despite its high ΔG_H, became highly catalytic towards the HER once lithiated into $LiTi_2O_4$ (as characterized by a low ΔG_H). This increased catalytic activity according to the degree of lithiation might explain why LTO in non-aqueous batteries effectively catalyzed the decomposition of trace H_2O present in electrodes and electrolyte. With a highly negative ΔG_H, ZnO would also serve as a good candidate for HER suppression. However, its high electronic conductivity accelerated the charge transfer between the electrolyte and electrodes, which kinetically favors the electrochemical reduction of water. Conversely, Al_2O_3 had a large bandgap (5.33 eV) (Fig. 1c), which suggested very poor electrical conductivity that prevented charge transfer, in sharp comparison with the bandgaps of lithiated $LiTi_2O_4$ (0 eV) and ZnO (1.48 eV), respectively. In fact, the latter two were well known for their metallic and semiconducting behaviors (Fig. 1d and S1†). Therefore, the insulator Al_2O_3 would be the best candidate surface for HER suppression.

An Al_2O_3 layer of nanometric thickness was coated on an LTO electrode using atomic layer deposition (ALD). As shown in the scanning electron microscope (SEM) image (Fig. 2a), LTO maintained the morphology and crystallinity of particles after coating. Energy dispersive X-ray (EDX) spectroscopy confirmed the existence of Al on the electrode surface. The uniform distribution of Al according to element mapping (Fig. 2b) revealed that the electrode surface was covered uniformly by Al_2O_3. The Al_{2p} peak at ~74.8 eV during X-ray photoelectron spectroscopy (XPS, Fig. 2c) was closely indexed to Al_2O_3. The thickness of the coating was determined to be ~3 nm by transmission electron microscopy (TEM) (Fig. 2d). An additional peak at ~350 cm^{-1} (ref. 38) during Raman spectroscopy (Fig. S2†) in comparison with pristine LTO also demonstrated the existence of Al_2O_3 coating.

The electrochemical performance of LTO electrodes coated with various materials was evaluated by linear sweep voltammetry (Fig. 3). Hydrogen evolution began at ~1.8 V *vs.* Li on the pristine LTO surface, which was higher than its lithiation potential (1.55 V). The HER process (rather than lithiation of LTO) dominated the cathodic reaction during the scan. The carbon coating enhanced the electronic conductivity of LTO, thus accelerating the HER (as evidenced by the higher currents and positively shifted HER potential). The TiO_2 coating also positively shifted the cathodic limit due to its high catalytic activity. In contrast, the ZnO coating and Al_2O_3 costing negatively shifted the cathodic limit potential by 0.1 V. In addition, the HER currents on the ZnO-coated and Al_2O_3-coated LTO electrode were much lower compared with those on pristine LTO. The capability of HER suppression as quantified by the

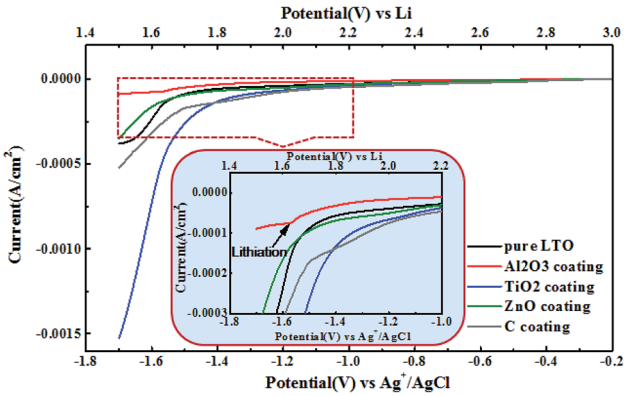

Fig. 3 Cathodic limits evaluated by linear sweep voltammetry on LTO surfaces coated with different materials (inset shows the enlarged view). Counter electrode: activated carbon; reference electrode: Ag/AgCl; scan rate: 1 mV s^{-1}.

onset potential of the HER should increase in the order TiO_2 < carbon < LTO < ZnO < Al_2O_3, which was consistent with the prediction in Fig. 1. The Al_2O_3 coating not only suppressed the HER catalytic activity but also acted as a kinetic barrier to slow down electron transfer from the electrode bulk to protons in the electrolyte.[39] Al_2O_3 coating shifted the HER potential to <1.5 V, so Li^+ intercalation was enabled before the HER, as evidenced by a sharp lithiation peak at 1.55 V (Fig. 4a). Using a similar approach, we also evaluated the effect of surface coating on the oxygen evolution reaction (OER). Al_2O_3 coating and TiO_2 coating on $LiNi_{0.5}Mn_{1.5}O_4$ reduced the side reactions on this high-voltage (4.8 V) cathode material only slightly (Fig. S3†).

As shown in the CV curves of Al_2O_3-coated LTO (Fig. 4a) and pristine LTO (Fig. S4†), an oxidative current peak at 1.8 V was clearly observed on the former, and it increased with cycling, whereas very low oxidation current was detected on pristine LTO. Therefore, Al_2O_3 coating on LTO effectively suppressed the HER, and Li^+ diffusion in Al_2O_3 was activated gradually during the initial few CV scans.[39–41]

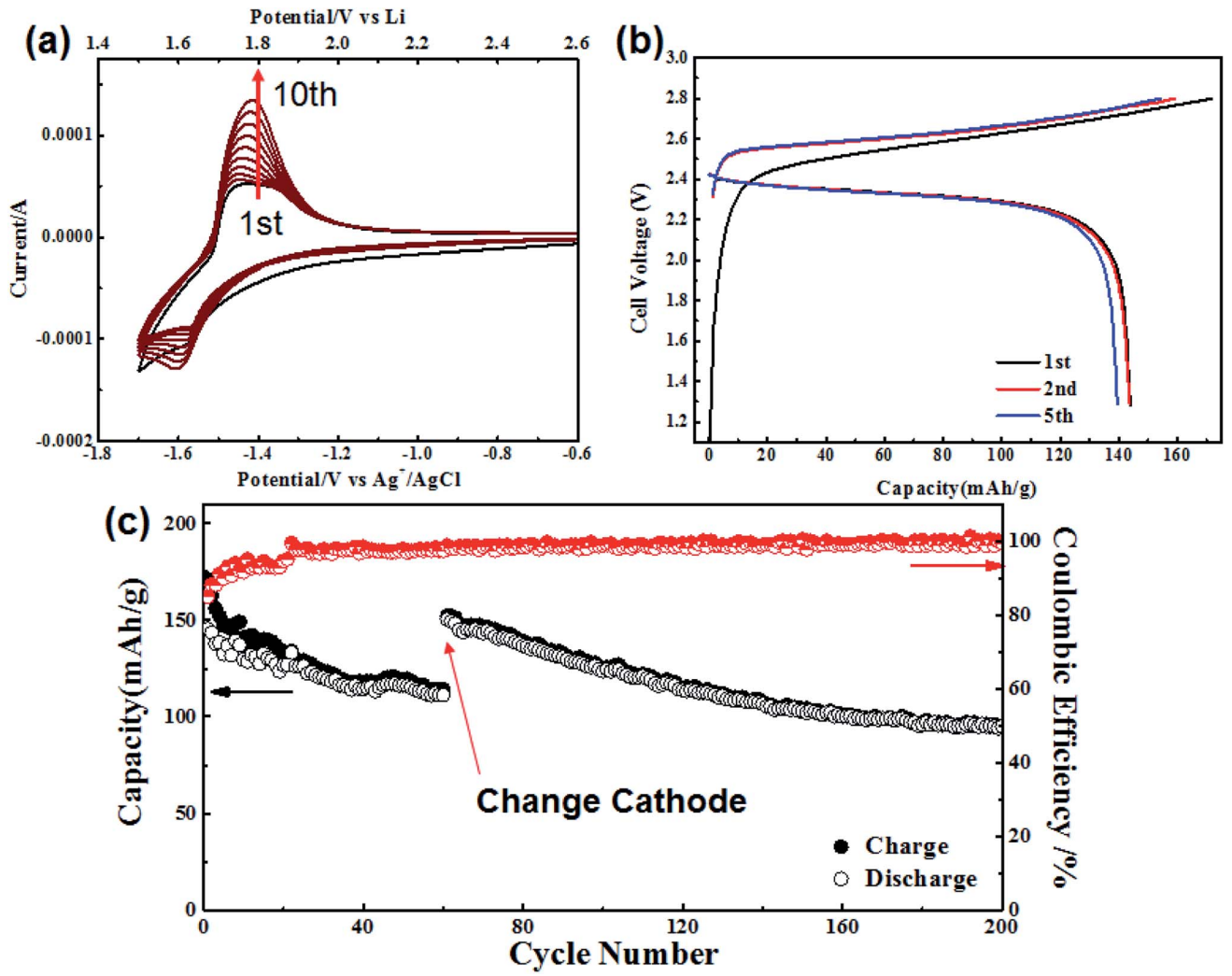

Fig. 4 (a) Cyclic voltammetry (CV) scan of Al_2O_3-coated LTO anodes in water-in-salt in electrolytes at the scanning rate of 5 mV s^{-1} using an activated carbon counter electrode and an Ag/AgCl reference electrode. (b) The voltage profile of the full cell using the Al_2O_3-coated LTO anode and LMO cathode at 1C current. (c) The cycling performance of the full cell using an Al_2O_3-coated LTO anode and LMO cathode.

$LiMn_2O_4$ (LMO) was used as a cathode to evaluate the electrochemical performance of Al_2O_3-coated LTO in the WiSE (Fig. S5†). The mass ratio of LMO : LTO was set as 2.5 : 1 to accommodate the low CE of LTO during the initial several cycles. 1C was used instead of a high rate to demonstrate the stability of the electrolyte in the full cell. Such LTO/LMO full cells delivered a voltage *plateau* at ~2.4 V during discharge. The discharging capacity based on LTO mass was 145 mA h g^{-1}. In the first cycle, a coulombic efficiency (CE) of 84.5% was delivered, indicating that a relatively small amount of electrolyte was consumed to form an additional LiF-rich SEI on the Al_2O_3-coated LTO anode. In comparison, pairing the uncoated LTO and LMO delivered a CE of 50% (Fig. S6†), further confirming the effect of the Al_2O_3 coating in suppressing the side reaction. As we reported previously, the reduction of salt anions bis(trifluoromethane sulfonyl)imide (TFSI) occurs between 1.9 V and 2.9 V.[4] Although reduction of TFSI anions is expected to occur if an Al_2O_3 coating is absent (Fig. S7†), formation of a complete SEI needs a long time (*i.e.*, few cycles in galvanostatic charge/discharge cycles). The lithiation potential of pristine LTO resides beyond the cathodic limit of the WiSE, so a significant HER will occur before lithiation. The persistent evolution of gas undoubtedly prevents complete formation of the SEI. For the initial cycles, when a robust SEI has not been constructed, protection of the Al_2O_3 surface serves as a key barrier to ensure that SEI chemistry occurs, and that the SEI ingredient formed from the reduction of the TFSI anion adheres to the anode surface. After the most challenging period in the initial cycles, a dense and complete SEI will come into shape (Fig. S7†), eventually providing long-term protection and allowing LTO to deliver a reversible capacity.

The cycling performance of the LTO/LMO full cell is shown in Fig. 4c. The capacity of the LTO/LMO full cell decreased gradually, whereas the CE increased from 84.5% to ~99% after 60 cycles. This decay should be induced by the persistent consumption of the Li source from LMO, as indicated by the low CE.[42] After taking apart the cycled cell and replenishing with a fresh LMO cathode, the cell capacity recovered to 150 mA h g^{-1} from 106 mA h g^{-1}. This result demonstrated that the capacity decay was due to excessive consumption of Li, whereas LTO itself was chemically stable in the aqueous electrolytes. Thus, the cycle performance could be extended to 200 cycles. More efficient surface passivation using new coating materials holds the potential for further optimization of the LTO electrode for superior performance.

In summary, we investigated how to suppress surface HER activity to enable the reversible lithiation/de-lithiation reactions of the LTO anode in aqueous electrolytes. Upon combining the simulation and experimental results, Al_2O_3 was identified to be an optimum surface-passivation material based on its high ΔG_H and low electronic conductivity. Dramatic improvement in electrochemical performance was realized with an Al_2O_3 coating on the LTO electrode *via* ALD. The Li-ion full cell constructed with LTO and LMO delivered a high working voltage of 2.4 V for 200 cycles. More importantly, we revealed the importance of the catalytic electrode surface in dictating the electrochemical stability of electrolyte materials. The work could also impact other aqueous or non-aqueous devices that face similar challenges.

Conflicts of interest

There are no conflicts to declare.

Acknowledgements

We acknowledge the support of the Maryland Nano Center and its NispLab. The latter is supported in part by the NSF as a MRSEC Shared Experimental Facility. C.-F. L. and G. W. R. are supported by Nanostructures for Electrical Energy Storage (NEES) funded by the U.S. Department of Energy, Office of Science, Office of Basic Energy Sciences (DESC0001160).

References

1 F. Wang, L. Suo, Y. Liang, C. Yang, F. Han, T. Gao, W. Sun and C. Wang, *Adv. Energy Mater.*, 2017, **7**, 1600922.
2 F. Wang, Y. Lin, L. Suo, X. Fan, T. Gao, C. Yang, F. Han, Y. Qi, K. Xu and C. Wang, *Energy Environ. Sci.*, 2016, **9**, 3666–3673.
3 W. Li, J. R. Dahn and D. S. Wainwright, *Science*, 1994, **264**, 1115–1118.
4 L. Suo, O. Borodin, T. Gao, M. Olguin, J. Ho, X. Fan, C. Luo, C. Wang and K. Xu, *Science*, 2015, **350**, 938–943.
5 Y. Yamada, K. Usui, K. Sodeyama, S. Ko, Y. Tateyama and A. Yamada, *Nat. Energy*, 2016, **1**, 16129.
6 J.-Y. Luo and Y.-Y. Xia, *Adv. Funct. Mater.*, 2007, **17**, 3877–3884.
7 L. Suo, O. Borodin, W. Sun, X. Fan, C. Yang, F. Wang, T. Gao, Z. Ma, M. Schroeder and A. von Cresce, *Angew. Chem., Int. Ed.*, 2016, **55**, 7136–7141.
8 L. Suo, O. Borodin, Y. Wang, X. Rong, W. Sun, X. Fan, S. Xu, M. Schroeder, A. Cresce, F. Wang, C. Yang, Y. Hu, K. Xu and C. Wang, *Adv. Energy Mater.*, 2017, **7**, 1701189.
9 L. Suo, D. Oh, y. lin, Z. Zhuo, O. Borodin, T. Gao, f. wang, A. Kushima, Z. Wang, H. Kim, Y. Qi, W. Yang, F. Pan, J. Li, K. Xu and C. Wang, *J. Am. Chem. Soc.*, 2017, **139**, 18670–18680.
10 F. Wang, O. Borodin, T. Gao, X. Fan, W. Sun, F. Han, A. Faraone, J. A. Dura, K. Xu and C. Wang, *Nat. Mater.*, 2018, **1**, 543–549.
11 F. Wang, O. Borodin, M. S. Ding, M. Gobet, J. Vatamanu, X. Fan, T. Gao, N. Edison, Y. Liang and W. Sun, *Joule*, 2018, **2**, 1–11.
12 C. Yang, J. Chen, T. Qing, X. Fan, W. Sun, A. von Cresce, M. S. Ding, O. Borodin, J. Vatamanu and M. A. Schroeder, *Joule*, 2017, **1**, 122–132.
13 M. Börner, S. Klamor, B. Hoffmann, M. Schroeder, S. Nowak, A. Würsig, M. Winter and F. Schappacher, *J. Electrochem. Soc.*, 2016, **163**, A831–A837.
14 M. Steinhauer, S. Risse, N. Wagner and K. A. Friedrich, *Electrochim. Acta*, 2017, **228**, 652–658.
15 Q. Zhang, J. Pan, P. Lu, Z. Liu, M. W. Verbrugge, B. W. Sheldon, Y.-T. Cheng, Y. Qi and X. Xiao, *Nano Lett.*, 2016, **16**, 2011–2016.

16 K. Xu, *Chem. Rev.*, 2014, **114**, 11503–11618.
17 K. Xu, *Chem. Rev.*, 2004, **104**, 4303–4417.
18 D. M. Seo, D. Chalasani, B. S. Parimalam, R. Kadam, M. Nie and B. L. Lucht, *ECS Electrochem. Lett.*, 2014, **3**, A91–A93.
19 X.-Y. Yue, X.-L. Li, W.-W. Wang, D. Chen, Q.-Q. Qiu, Q.-C. Wang, X.-J. Wu, Z.-W. Fu, Z. Shadike and X.-Q. Yang, *Nano Energy*, 2019, **60**, 257–266.
20 Y. Liu, D. Lin, P. Y. Yuen, K. Liu, J. Xie, R. H. Dauskardt and Y. Cui, *Adv. Mater.*, 2017, **29**, 1605531.
21 N. W. Li, Y. X. Yin, C. P. Yang and Y. G. Guo, *Adv. Mater.*, 2016, **28**, 1853–1858.
22 M. Gauthier, T. J. Carney, A. Grimaud, L. Giordano, N. Pour, H. H. Chang, D. P. Fenning, S. F. Lux, O. Paschos, C. Bauer, F. Maglia, S. Lupart, P. Lamp and Y. Shao-Horn, *J. Phys. Chem. Lett.*, 2015, **6**, 4653–4672.
23 K. Wongrujipairoj, L. Poolnapol, A. Arpornwichanop, S. Suren and S. Kheawhom, *Phys. Status Solidi B*, 2017, **254**, 1600442.
24 H. He, H. Tong, X. Song, X. Song and J. Liu, *J. Mater. Chem. A*, 2020, **8**, 7836–7846.
25 Y.-D. Cho and G. T.-K. Fey, *J. Power Sources*, 2008, **184**, 610–616.
26 Y. Zhang, Y. Wu, W. You, M. Tian, P. W. Huang, Y. Zhang, Z. Sun, Y. Ma, T. Hao and N. Liu, *Nano Lett.*, 2020, **20**, 4700–4707.
27 P. Quaino, F. Juarez, E. Santos and W. Schmickler, *Beilstein J. Nanotechnol.*, 2014, **5**, 846–854.
28 Y. Fujimori, W. E. Kaden, M. A. Brown, B. Roldan Cuenya, M. Sterrer and H.-J. Freund, *J. Phys. Chem. C*, 2014, **118**, 17717–17723.
29 T. F. Jaramillo, K. P. Jørgensen, J. Bonde, J. H. Nielsen, S. Horch and I. Chorkendorff, *science*, 2007, **317**, 100–102.
30 J. Greeley, T. F. Jaramillo, J. Bonde, I. B. Chorkendorff and J. K. Norskov, *Nat. Mater.*, 2006, **5**, 909–913.
31 B. Conway and B. Tilak, *Electrochim. Acta*, 2002, **47**, 3571–3594.
32 B. Conway and G. Jerkiewicz, *Solid State Ionics*, 2002, **150**, 93–103.
33 L. Scatena, M. Brown and G. Richmond, *Science*, 2001, **292**, 908–912.
34 M. Jaksic, *J. New Mater. Electrochem. Syst.*, 2000, **3**, 153–168.
35 J. Barber, S. Morin and B. Conway, *J. Electroanal. Chem.*, 1998, **446**, 125–138.
36 F. Han, Y. Zhu, X. He, Y. Mo and C. Wang, *Adv. Energy Mater.*, 2016, **6**, 1501590.
37 D. Strmcnik, P. P. Lopes, B. Genorio, V. R. Stamenkovic and N. M. Markovic, *Nano Energy*, 2016, **29**, 29–36.
38 Y. Liu, B. Cheng, K.-K. Wang, G.-P. Ling, J. Cai, C.-L. Song and G.-R. Han, *Solid State Commun.*, 2014, **178**, 16–22.
39 K. Leung, Y. Qi, K. R. Zavadil, Y. S. Jung, A. C. Dillon, A. S. Cavanagh, S. H. Lee and S. M. George, *J. Am. Chem. Soc.*, 2011, **133**, 14741–14754.
40 Y. Hu, A. Ruud, V. Miikkulainen, T. Norby, O. Nilsen and H. Fjellvåg, *RSC Adv.*, 2016, **6**, 60479–60486.
41 S.-Y. Kim, A. Ostadhossein, A. C. Van Duin, X. Xiao, H. Gao and Y. Qi, *Phys. Chem. Chem. Phys.*, 2016, **18**, 3706–3715.
42 X.-Y. Yue, W.-W. Wang, Q.-C. Wang, J.-K. Meng, X.-X. Wang, Y. Song, Z.-W. Fu, X.-J. Wu and Y.-N. Zhou, *Energy Storage Materials*, 2019, **21**, 180–189.

